



Original article

Synthesis and anti-inflammatory evaluation of novel mono-carbonyl analogues of curcumin in LPS-stimulated RAW 264.7 macrophages

Chengguang Zhao^{a,1}, Yuepiao Cai^{a,1}, Xuzhi He^a, Jianling Li^a, Li Zhang^a, Jianzhang Wu^{a,b}, Yunjie Zhao^a, Shulin Yang^b, Xiaokun Li^a, Wulan Li^{c,**}, Guang Liang^{a,b,*}

^aSchool of Pharmacy, Wenzhou Medical College, 1210 College Town, Wenzhou, Zhejiang 325035, China

^bCollege of Chemical Engineering, Nanjing University of Science and Technology, 200 Xiaolingwei St., Nanjing, Jiangsu 210094, China

^cCollege of Mathematics and Computer Science, Hunan Normal University, Changsha, Hunan 410081, China

ARTICLE INFO

Article history:

Received 13 August 2010

Received in revised form

11 September 2010

Accepted 16 September 2010

Available online 8 October 2010

Keywords:

Curcumin

Mono-carbonyl analogues

QSAR

TNF- α

IL-6

Anti-inflammation

ABSTRACT

Curcumin is a multifunctional natural product with regulatory effects on inflammation. However, a major limitation for the application of curcumin is its poor bioavailability. We previously demonstrated that the mono-carbonyl analogues of curcumin possessed improved pharmacokinetic profiles. In this study, 33 novel mono-carbonyl analogues of curcumin were synthesized and their inhibition against TNF- α and IL-6 release was evaluated in LPS-stimulated RAW 264.7 macrophages. Based on the screening data, quantitative structure–activity relationship was conducted, indicating that electron-withdrawing groups in benzene ring are favourable to anti-inflammatory activities of B-class compounds. Furthermore, compounds **AN1** and **B82** demonstrated anti-inflammatory abilities in a dose-dependent manner. These raise the possibility that these compounds might serve as potential agents for the treatment of inflammatory diseases.

© 2010 Elsevier Masson SAS. All rights reserved.

1. Introduction

Curcumin (diferuloylmethane) is an orange–yellow and dietary polyphenolic phytochemical in turmeric (*Curcuma longa*). In the past decades, curcumin has been shown to exhibit antioxidant, anti-inflammatory, antiviral, antibacterial, and thus has a potential against various malignant cancers, diabetes, allergies, arthritis and other chronic illnesses [1–6]. These effects have been proved to be mediated through the regulation of various transcriptional factors, inflammatory cytokines and other enzymes [7–10]. This molecule is under clinical trials for cancer preventive drug development and for the treatment of rheumatoid arthritis and infectious diseases [11–14].

Although curcumin has been shown to be safe and modulates several targets that have been linked with cancer and various other

chronic diseases, its efficacy in clinic has been limited by its poor bioavailability and fast metabolism *in vivo* [15,16]. For example, with oral administration at the dose of 450–3600 mg/day in a phase I trial, the blood concentration of curcumin in plasma and target tissues is under the detection limit [17]. Curcumin seems to be metabolized and degraded through reduction. It is believed from recent studies that the β -diketone moiety in the structure of curcumin appears to be a specific substrate of a series of aldo–keto reductases and can be decomposed rapidly *in vivo* [18,19]. Some of analogues without the β -diketone moiety have been designed and yielded in our previous study, and as expected, they have been demonstrated to possess enhanced stability *in vitro* and improved pharmacokinetic profiles *in vivo* [20].

Proinflammation is involved in many different pathophysiological disease processes, and the inflammatory conditions may serve as an important and common pattern in various diseases including cardiovascular diseases and cancer [21–23]. Numerous cytokines are present with proinflammation. For example, TNF- α and IL-6 are the two proinflammatory cytokines involved in the pathogenesis of hemodialysis-related (cardiovascular) diseases [24,25]. Therapeutic candidates targeting proinflammatory cytokines or inhibiting the over-expressions of cytokines become a focus of novel drug development for inflammatory disease,

* Corresponding author. Bioorganic & Medicinal Chemistry Research Center, School of Pharmacy, Wenzhou Medical College, 1210 College Town, Wenzhou, Zhejiang 325035, China. Tel.: +86 577 86699892; fax: +86 577 86689983.

** Corresponding author.

E-mail addresses: wulanli2009@163.com (W. Li), cuiliang1234@163.com (G. Liang).

¹ These authors contribute equally to this work.

cancer, diabetes and cardiovascular disease [26–28]. With respect to inflammatory cytokines *in vitro*, curcumin and its derivatives have been shown to down-regulate expression of several cytokines, including TNF- α , IL-1, IL-6, and IL-12 by inhibiting the activation of free radical-activated transcription factors, such as nuclear factor- κ B and AP-1 [29–31].

Previously, we have evaluated a part of mono-carbonyl analogues of curcumin for anti-inflammatory properties using lipopolysaccharide (LPS)-stimulated mouse macrophages and discussed the primary structure–activity relationship (SAR) [32,33]. As part of our ongoing research for potential anti-inflammatory drug candidates, in this study, we further presented 33 newly synthesized mono-carbonyl analogues of curcumin and their quantitative SAR analysis for their anti-inflammatory activities in mouse RAW 264.7 macrophages. Following initial examination, we then showed that the best two compounds can prevent LPS-induced inflammation in a dose-dependent manner.

2. Result and discussion

2.1. Chemistry

As reported previously [20], the deletion of the central β -diketone may improve pharmacokinetic profiles of curcumin derivatives.

Therefore, three series of 5-carbon linker-containing mono-carbonyl analogues of curcumin, 1,5-diaryl-1,4-pentadiene-3-ones (B), together with cyclopentanone (A) and cyclohexanone (C) analogues, were designed by displacing β -diketone moiety with a single carbonyl group. The same methodology as previously reported was used to carry out the synthesis of new compounds here [20,33]. Different substituents with opposing electronic properties in the benzene rings were designed to investigate and discuss the structure–activity relationship. The synthesis and structures of compounds **N1–4** and **76–88** were shown in Fig. 1. The synthesis essentially involved an aldol condensation of the appropriate aromatic aldehyde with cyclohexanone, cyclopentanone or acetone in an alkaline medium at room temperature, respectively. Generally, the coupling reaction yielded the respective products in high yields (50–91%). The diaryl structure was confirmed by the absence of methyl protons adjacent to the carbonyl group in the ^1H NMR spectra of A-class compounds and the absence of two methylene protons near to the central carbonyl in the spectra of B and C-class compounds.

2.2. Inhibitory screening against LPS-induced TNF- α and IL-6 release

TNF- α and IL-6 are two of well characterized cytokines that play an important role in many inflammatory diseases caused by

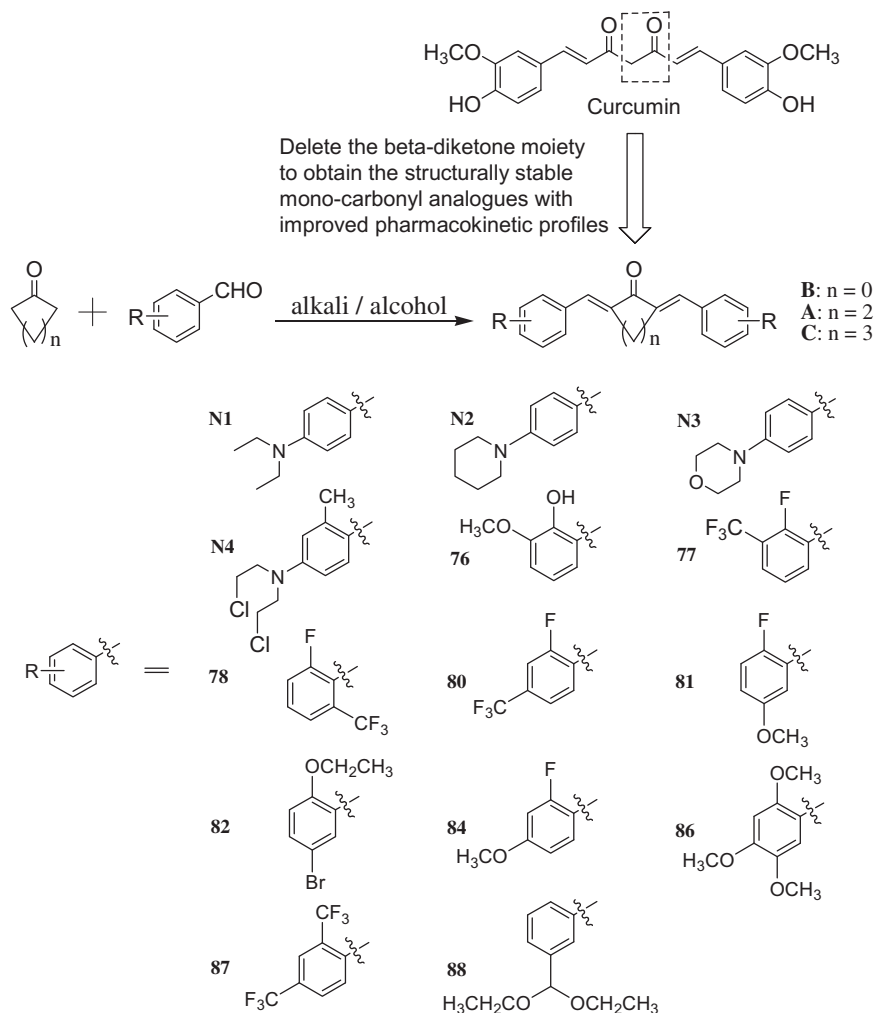


Fig. 1. Chemical structure of curcumin and the design of its mono-carbonyl analogues as well as general synthesis and chemical structures of mono-carbonyl analogues of curcumin.

endotoxins produced by Gram-negative bacteria. Over-expression of TNF- α and IL-6 contributes significantly to the pathological complications observed in various diseases [24,25]. TNF- α and IL-6 are produced mainly in cells of reticuloendothelial origin (e.g., macrophages), especially when induced by many external stimuli, such as lipopolysaccharide (LPS), a component of the cell wall of Gram-negative bacteria.

Curcumin and its 33 synthetic analogues were evaluated for their ability to inhibit the TNF- α and IL-6 release in RAW 264.7 mouse macrophages stimulated by LPS. Macrophages were stimulated with LPS in the presence or absence of the compounds at a concentration of 10 μ M, where the leading compound curcumin showed a significant inhibition against TNF- α and IL-6 production. The cells were pre-incubated for 60 min with curcumin analogues and DMSO as a control. After that, cells were treated with LPS (0.5 μ g/ml) for 22 min at 37 $^{\circ}$ C. The amount of TNF- α and IL-6 in media was detected through enzyme-linked immunosorbent assay (ELISA) and normalized by protein concentration of cells harvested in homologous culture plates.

Fig. 2 gave the results of the anti-inflammatory evaluation of curcumin and three analogue classes. Curcumin reduced LPS-mediated TNF- α and IL-6 expression at 35.6% and 75.7%, respectively. Among these 33 compounds, the majority of the tested compounds inhibited LPS-induced TNF- α and IL-6 expression to various degrees. Compounds **AN1**, **AN4**, **CN3**, **B78**, and **B82** exhibited higher inhibitory ability than the leading curcumin (35.6%) against LPS-induced TNF- α expression. Compounds **AN2**, **BN3**, **BN4**, **A78**, **A84**, **B84**, **B86**, **C77**, **C81** and **C87** showed inhibition of TNF- α production in a range of 20–35.6%. With regard to IL-6, substituted amino-containing analogues **BN1**–**3** showed inhibition of IL-6 over 50% compared to the LPS-treated control. Compounds **B82** and **B86** exhibited comparable activity to curcumin against IL-

6 release and **B84** also showed 51.1% inhibition of IL-6. Furthermore, compounds **AN4**, **BN4**, **A81**, and **B78** showed more than 30% inhibitory effects against IL-6 expression compared to LPS control. Compounds **AN1** and **B82**, especially, were more potent than curcumin at the same concentration in inhibiting LPS-induced TNF- α and IL-6 expression. Among the tested compounds, **AN1** showed the strongest inhibitory effect on LPS-induced TNF- α and IL-6 release and its inhibitory rates reached 67.5 and 92.7%, respectively, compared to the LPS control.

Chemical modifications as well as the synthesis of the curcumin analogues have been tried by many research groups to find out the SAR conclusion and better leads for the treatment of inflammatory diseases. However, few significantly potent analogues were found to be under final considerations as a drug. Concurrently, 33 monocarbonyl analogues were synthesized and their inhibitory effects on TNF- α and IL-6 release were evaluated. As reported previously, it is observed here that acetone-derived B-class analogues are more effective, especially against LPS-induced IL-6 expression, than cyclopentanone-derived A-class and cyclohexanone-derived C-class analogues, indicating that the structure of a 5-carbonyl linker may play a role on such activities. However, **AN1** was claimed the strongest inhibition against LPS-induced IL-6 release. The detailed rationale is unclear yet. Some special conformation, not molecular structure, of **AN1** may contribute to its strong bioactivity.

2.3. Quantitative structure–activity relationship

To further demonstrate the SAR of B-class compounds and to evaluate the effects of various substituents on the activity, QSARs were calculated on the nine B-class compounds. The relative amounts of TNF- α and IL-6 expression in screening section were used as the factors of biological activity, named as $RAC_{TNF-\alpha}$ and

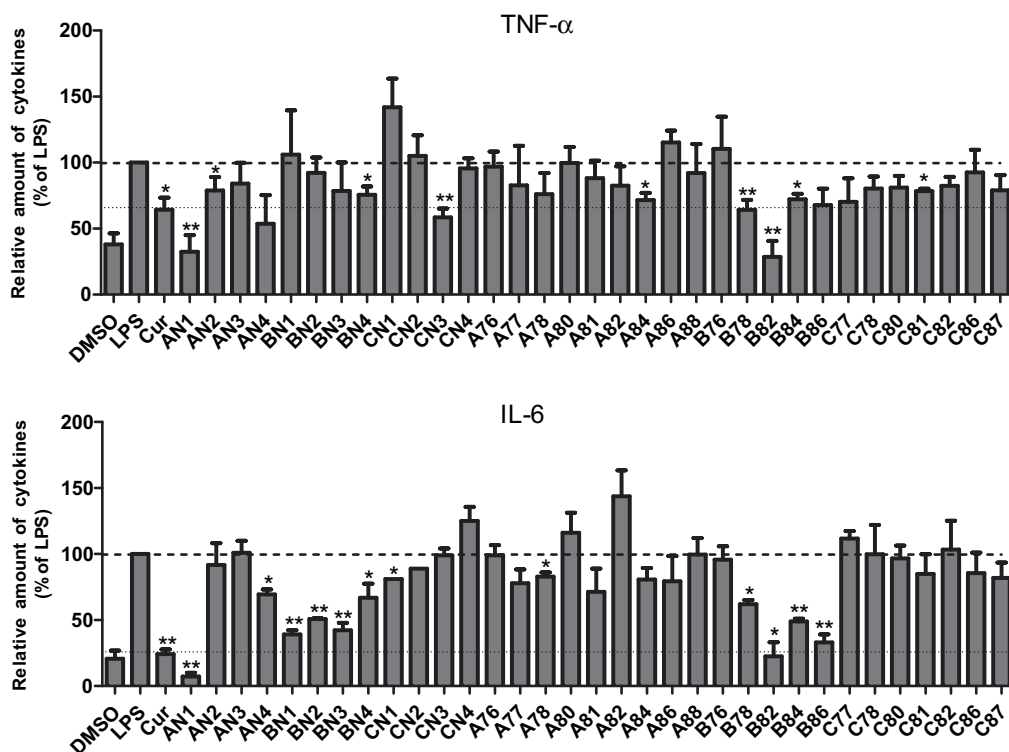


Fig. 2. Curcumin and its analogues inhibited LPS-induced TNF- α and IL-6 secretion in RAW 264.7 macrophages. Macrophages were plated at a density of 4.0×10^5 /plate for overnight in 37 $^{\circ}$ C and 5% CO₂. Cells were pre-treated with curcumin or its analogues (10 μ M) for 2 h, then treated with LPS (0.5 μ g/ml) for 22 h. TNF- α and IL-6 levels in the culture media were measured by ELISA and were normalized by the total protein. The results were expressed as the percent of LPS control. Each bar represents mean \pm SE of 3–5 independent experiments. Statistical significance relative to LPS was indicated, * p < 0.05, ** p < 0.02.

RAC_{IL-6}, respectively. $\log(1/\text{RAC}_{\text{TNF-}\alpha})$ and $\log(1/\text{RAC}_{\text{IL-6}})$ were used as the dependent variables in the linearization procedure. To construct QSAR model, various types of parameters are operated, including the quantum-chemical descriptors calculated by density functional theory (DFT) method, molar refractivity and the coefficient of molecular partition octanol–water ($\log P$) which reflects the molecular properties, and topological descriptors including kappa index, Zagreb index and Wiener index. A good correlation was observed with some quantum chemical descriptors for B-class compounds. However, most of the parameters have to be disregarded due to the low correlation to the biological activity, such as electrostatic potential (EP), HOMO and LUMO energies, molecular dipole moment (MDP) and molecular polarizability (MP), molar refractivity, $\log P$. The calculated values of the quantum chemical descriptors are shown in Table S1 (see Table S1 in Supporting material).

Multiple linear regressions between the different activities of B-class derivatives and the quantum chemical descriptors were studied, and the QSAR equations (shown as Eq. (1) and Eq. (2) in Fig. 3) with the largest correlation coefficient were obtained. As illustrated in Fig. 3A, the Eq. (1) has high quality and the parameters used in this equation can explain the variance in the RAC_{TNF- α} activity of B-class derivatives. Eq. (1) satisfactorily describes the

correlation between the biological activity and different substituted groups. The model involves the DFT-calculated q_π and SDN-sub, which mean the sum of π -electron densities of the whole molecules and the sum of nucleophilic superdelocalizabilities of the substituent moiety, respectively. These parameters are frequently employed to characterize molecular interactions and can be used to compare corresponding atoms in different molecules. This equation indicates that the electronic properties play an important role in the anti-TNF- α properties of B-class compounds. The correlation analysis shows that q_π correlates $\log(1/\text{RAC}_{\text{TNF-}\alpha})$ at the significance level of 0.0004, with correlation coefficient of -0.744 in this model. Negative coefficient of q_π indicates that electron-withdrawing substituents would benefit the activity.

The correlation analysis between anti-IL-6 activities of B-class compounds and their quantum chemical descriptors is illustrated in Fig. 3B. Eq. (2) suggests that net atomic charge on the carbon atom numbered 3 and the oxygen atom numbered 8 in B-class compounds are important parameters influencing the RAC_{IL-6} activity. It has been proven that local electron densities or charges are important in many chemical reactions and physico-chemical properties of compounds. Mulliken atomic charges of the C-3 and O-8 atom were calculated at B3LYP/6-31G level of theory. In most cases the presence of donor and acceptor groups in aromatic ring has a direct influence on the charge of this C atom and O atom. Although this equation gives a relatively modest correlation with R^2 of 0.71, the QSAR conclusion is coincident to RAC_{TNF- α} analysis of these compounds. The calculated correlation coefficient between $Q_{\text{C}3}$ and $\log(1/\text{RAC}_{\text{IL-6}})$ is -0.736 , which indicates that electron-withdrawing group is favourable because it will decrease the electrophilicity of C-3 and increase the biological activity.

2.4. AN1 and B82 inhibit TNF- α and IL-6 release in a dose-dependent manner

Among the active analogues above, two compounds, **AN1** and **B82**, which demonstrated the highest activities and low cytotoxicity (data not shown) in macrophages, were chosen for further evaluation of their dose-dependent inhibitory effects against LPS-induced TNF- α and IL-6 release. RAW 264.7 macrophages were pre-treated with **AN1** or **B82** in a series of concentrations (1, 2.5, 5.0, 10 and 20 μM) for 2 h and were subsequently incubated with LPS (0.5 $\mu\text{g}/\text{ml}$) for 22 h. As shown in Fig. 4, our data demonstrated a dose-dependent inhibition of LPS-induced TNF- α and IL-6 release by **AN1** and **B82**. Accordingly, the IC_{50} values of these two compounds are determined and listed in Fig. 4. **AN1** exhibited the lowest IC_{50} value (1.07 μM) when inhibiting IL-6 release. The inhibition of TNF- α and IL-6 release by **AN1** and **B82** in a dose-dependent manner, suggests the potential of these compounds as anti-inflammatory agents.

Combined with our previous studies [20], it is further confirmed that these mono-carbonyl analogues without β -diketone may render themselves favorably to the development of promising curcumin-based anti-inflammatory drugs from both pharmacokinetic and pharmacological standpoints. Further studies including analysis of the design of novel B-class compounds with electron-withdrawing substituents and investigation of the underlying molecular mechanisms of these active compounds at the transcriptional or posttranscriptional level are necessary to further establish this investigational pathway.

3. Conclusion

In summary, we presented a series of novel 5-carbon linker-containing mono-carbonyl analogues of curcumin and evaluated their potent inhibitory activities against LPS-induced TNF- α and

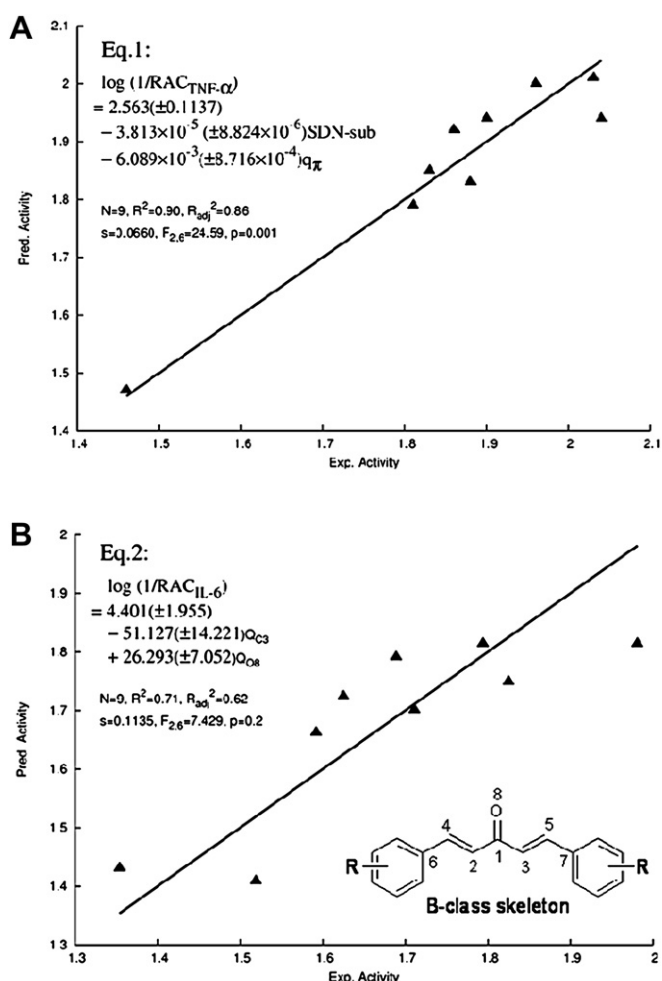


Fig. 3. Plot of predicted activity against the corresponding experimental activity. N , the number of compounds taken into account in the regression; R^2 , the multiple correlation coefficient; R_{adj}^2 , adjusted multiple correlation coefficient; s , residual standard error; F value is related to the F-statistic analysis (Fischer test). The numbers in parentheses mean the standard deviation of the coefficients.

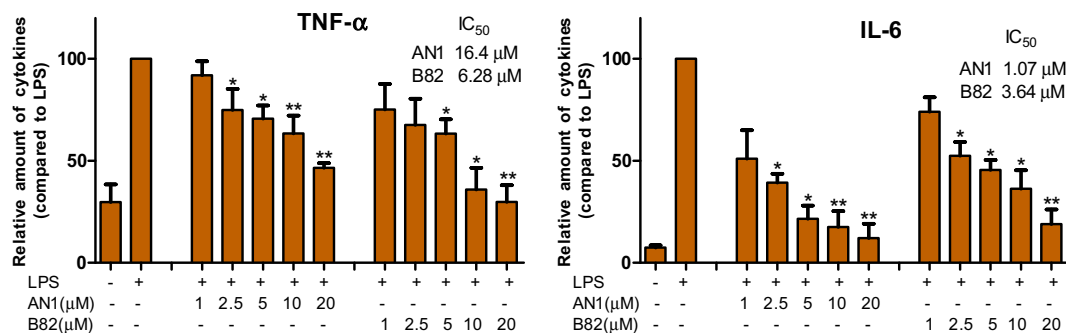


Fig. 4. AN1 and B82 inhibited LPS-induced TNF- α and IL-6 release in a dose-dependent manner in RAW 264.7 macrophages. Macrophages were plated at a density of 4.0×10^6 /plate overnight in 37 °C and 5% CO₂. Cells were pre-treated with specific compounds as indicated for 2 h, followed by LPS (0.5 μ g/ml) treatment for 22 h. TNF- α and IL-6 levels in the culture media were measured by ELISA and were normalized to the total protein amount. The results are expressed as percent of LPS control. Each bar represents mean \pm SE of 3–5 independent experiments. Statistical significance relative to LPS is indicated, * $p < 0.05$; ** $p < 0.01$.

IL-6 release in RAW 264.7 macrophages. It was concluded that acetone-derived B-class analogues are more effective than cyclopentanone-derived A-class and cyclohexanone-derived C-class analogues. Combined with the QSAR analysis, electron-withdrawing groups in benzene ring are favourable to anti-inflammatory activities of B-class compounds. Compounds **AN1** and **B82** were the most potent analogues and exhibited anti-inflammatory abilities in a dose-dependent manner in macrophages. This presents the possibility that mono-carbonyl analogues of curcumin might serve as potential agents for the treatment of various inflammatory diseases.

4. Experimental section

4.1. General procedure for the synthesis of compounds

All reagents for syntheses were obtained from Sigma–Aldrich and Fluka, and were used without purification. Thin-layer chromatography (TLC) was performed on Kieselgel 60 F₂₅₄ plates. Melting points were determined on a Fisher-Johns melting apparatus and were uncorrected. ¹H NMR spectra were recorded on a Bruker 600 MHz instruments. The chemical shifts were presented in terms of parts per million with TMS as the internal reference. Electron-spray ionization mass spectra in positive mode (ESI-MS) data were recorded on a Bruker Esquire 3000⁺ spectrometer. Column chromatography purifications were carried out on Silica Gel 60 (E. Merck, 70–230 mesh).

Briefly, an amount of 7.5 mmol acetone (B-class), cyclopentanone (A-class), or cyclohexanone (C-class) was added to a solution of 15 mmol arylaldehyde in MeOH (10 ml). The solution was stirred at room temperature for 20 min, followed by dropwise addition of NaOCH₃/CH₃OH (1.5 ml, 7.5 mmol). The mixture was stirred at room temperature and monitored with TLC. When the reaction was finished, the residue was poured into saturated NH₄Cl solution and filtered. The precipitate was washed with water and cold ethanol, and dried in vacuum. The solid was purified by chromatography over silica gel using CH₂Cl₂/CH₃OH as the eluent to yield compounds [34].

4.1.1. (2E,5E)-2,5-Bis(2-hydroxy-3-methoxybenzylidene)cyclopentanone (**A76**)

Green powder, 61.2% yield, mp 120.1–122.7 °C. ¹H NMR (CDCl₃) δ : 7.74 (2H, s, Ar–CH=C \times 2), 7.19 (2H, m, Ar–H⁶ \times 2), 7.13 (2H, m, Ar–H⁵ \times 2), 6.98 (2H, m, Ar–H⁴ \times 2), 5.35 (2H, s, Ar–OH \times 2), 3.96 (6H, s, Ar–O–CH₃ \times 2), 2.78 (4H, s, CH₂–CH₂). ESI-MS m/z : 351.2 (M – H)[–], calcd for C₂₂H₁₄F₈O: 352.38.

4.1.2. (2E,5E)-2,5-Bis(2-fluoro-3-(trifluoromethyl)benzylidene)cyclopentanone (**A77**)

Yellow powder, 58.1% yield, mp 221.8–222.4 °C [223 °C, lit. [34]]. ESI-MS m/z : 433.1 (M + H)⁺, calcd for C₂₁H₁₂F₈O: 432.31.

4.1.3. (2E,5E)-2,5-Bis(2-fluoro-6-(trifluoromethyl)benzylidene)cyclopentanone (**A78**)

Yellow powder, 50.4% yield, mp 95.4–97.9 °C. ¹H NMR (CDCl₃) δ : 7.64 (2H, s, Ar–CH=C \times 2), 7.47 (2H, d, $J = 8.4$ Hz, Ar–H⁵ \times 2), 7.44–7.47 (2H, d, $J = 8.4$ Hz, Ar–H⁴ \times 2), 7.33–7.35 (2H, t, $J = 9.0$ Hz, Ar–H³ \times 2), 2.60 (4H, s, CH₂–CH₂). ESI-MS m/z : 433.3 (M + H)⁺, 455.1 (M + Na)⁺, calcd for C₂₁H₁₂F₈O: 432.31.

4.1.4. (2E,5E)-2,5-Bis(2-fluoro-4-(trifluoromethyl)benzylidene)cyclopentanone (**A80**)

Yellow powder, 86.4% yield, mp 164.7–169.5 °C. ¹H NMR (CDCl₃) δ : 7.77 (2H, s, Ar–CH=C \times 2), 7.68 (2H, t, $J = 7.5$ Hz, Ar–H⁵ \times 2), 7.48 (2H, d, $J = 8.4$ Hz, Ar–H⁶ \times 2), 7.41 (2H, d, $J = 8.4$ Hz, Ar–H³ \times 2), 3.07 (2H, s, CH₂–CH₂). ESI-MS m/z : 432.8 (M + H)⁺, calcd for C₂₁H₁₂F₈O: 432.31.

4.1.5. (2E,5E)-2,5-Bis(2-fluoro-5-methoxybenzylidene)cyclopentanone (**A81**)

Yellow powder, 69.6% yield, mp 175.6–176.7 °C. ¹H NMR (CDCl₃) δ : 7.76 (2H, s, Ar–CH=C \times 2), 7.04–7.07 (4H, m, Ar–H^{3,4} \times 2), 6.88–6.90 (2H, m, Ar–H⁶ \times 2), 3.82 (6H, s, Ar–OCH₃ \times 2), 3.05 (4H, s, CH₂–CH₂). ESI-MS m/z : 357.2 (M + H)⁺, calcd for C₂₁H₁₈F₂O₃: 356.36.

4.1.6. (2E,5E)-2,5-Bis(5-bromo-2-ethoxybenzylidene)cyclopentanone (**A82**)

Yellow powder, 94.5% yield, mp 202.1–203.5 °C. ¹H NMR (CDCl₃) δ : 7.90 (2H, s, Ar–CH=C \times 2), 7.59 (2H, d, $J = 2.4$ Hz, Ar–H⁶ \times 2), 7.41 (2H, dd, $J = 2.4$ Hz, $J = 9.0$ Hz, Ar–H⁴ \times 2), 6.80 (2H, d, $J = 9.0$ Hz, Ar–H³ \times 2), 4.07 (4H, m, O–CH₂ \times 2), 3.02 (4H, s, CH₂–CH₂), 1.45 (6H, m, CH₃ \times 2). ESI-MS m/z : 507.1 (M + H)⁺, calcd for C₂₃H₂₂Br₂O₃: 506.23.

4.1.7. (2E,5E)-2,5-Bis(2-fluoro-4-methoxybenzylidene)cyclopentanone (**A84**)

Yellow powder, 41.7% yield, mp 179.1–181.9 °C. ¹H NMR (CDCl₃) δ : 7.76 (2H, s, Ar–CH=C \times 2), 7.53 (2H, t, $J = 8.4$ Hz, Ar–H⁶ \times 2), 6.75 (2H, d, $J = 8.4$ Hz, Ar–H⁵ \times 2), 6.67 (2H, d, $J = 12$ Hz, Ar–H³ \times 2), 3.84 (6H, s, Ar–OCH₃ \times 2), 3.02 (4H, s, CH₂–CH₂). ESI-MS m/z : 357.2 (M + H)⁺, calcd for C₂₁H₁₈F₂O₃: 356.36.

4.1.8. (2E,5E)-2,5-Bis(2,4,5-trimethoxybenzylidene)cyclopentanone (**A86**)

Orange powder, 92.6% yield, mp 225.8–227.1 °C. ¹H NMR (CDCl₃) δ : 7.97 (2H, s, Ar–CH=C \times 2), 7.13 (2H, s, Ar–H⁶ \times 2), 6.54

(2H, s, Ar–H³ × 2), 3.94 (6H, s, Ar²–OCH₃ × 2), 3.88 (12H, s, Ar^{4,5}–OCH₃ × 2), 3.06 (4H, s, CH₂–CH₂). ESI-MS *m/z*: 441.8 (M + H)⁺, calcd for C₂₅H₂₈O₇: 440.49.

4.1.9. (2*E*,5*E*)-2,5-Bis(3-(diethoxymethyl)benzylidene)cyclopentanone (**A88**)

Yellow powder, 95.5% yield, mp 84.4–85.1 °C. ¹H NMR (CDCl₃) δ: 8.10 (2H, s, Ar–CH=C × 2), 7.91 (2H, d, *J* = 7.8 Hz, Ar–H⁴ × 2), 7.85 (2H, d, *J* = 7.8 Hz, Ar–H⁵ × 2), 7.62–7.66 (4H, m, Ar–H^{2,6} × 2), 5.56 (2H, s, Ar–CH–O × 2), 3.72 (8H, m, O–CH₂ × 4), 3.18 (4H, s, CH₂–CH₂), 1.26 (12H, m, CH₃ × 4). ESI-MS *m/z*: 466.1 (M + H)⁺, calcd for C₂₉H₃₆O₅: 464.59.

4.1.10. (2*E*,5*E*)-2,5-Bis(4-(diethylamino)benzylidene)cyclopentanone (**AN1**) [35]

Red powder, 89.3% yield, mp 168.5–170.9 °C. ESI-MS *m/z*: 403.4 (M + H)⁺, calcd for C₂₇H₃₄N₂O: 402.57.

4.1.11. (2*E*,5*E*)-2,5-Bis(4-(piperidin-1-yl)benzylidene)cyclopentanone (**AN2**)

Brick red powder, 92.9% yield, mp 256.7–258.2 °C [260–262 °C, lit. [36]]. ESI-MS *m/z*: 427.3 (M + H)⁺, calcd for C₂₉H₃₄N₂O: 426.59.

4.1.12. (2*E*,5*E*)-2,5-Bis(4-morpholinobenzylidene)cyclopentanone (**AN3**)

Orange powder, 94.6% yield, mp 270–272 °C [275–277 °C, lit. [36]]. ESI-MS *m/z*: 431.3 (M + H)⁺, calcd for C₂₇H₃₀N₂O₃: 430.5.

4.1.13. (2*E*,6*E*)-2,6-Bis(4-(bis(2-chloroethyl)amino)benzylidene)cyclohexanone (**AN4**)

Yellow powder, 95.5% yield, mp 181.4–185.1 °C. ¹H NMR (CDCl₃) δ: 7.58 (4H, d, *J* = 9.0 Hz, Ar–H^{2,6} × 2), 7.54 (2H, s, Ar–CH=C × 2), 6.76 (4H, d, *J* = 9.0 Hz, Ar–H^{3,5} × 2), 3.83 (8H, t, *J* = 7.2 Hz, N–CH₂ × 4), 3.71 (8H, t, *J* = 7.2 Hz, Cl–CH₂ × 4), 3.10 (4H, s, CH₂–CH₂). ESI-MS *m/z*: 541.1 (M + H)⁺, calcd for C₂₇H₃₀Cl₄N₂O: 540.35.

4.1.14. (1*E*,4*E*)-1,5-Bis(2-hydroxy-3-methylphenyl)penta-1,4-dien-3-one (**B76**)

Green powder, 78.9% yield, mp 109.3–112.7 °C. ¹H NMR (CDCl₃) δ: 7.43 (2H, d, *J* = 16.2 Hz, Ar–CH=C × 2), 7.19 (2H, d, *J* = 7.8 Hz, Ar–H⁶ × 2), 7.12 (2H, d, *J* = 7.8 Hz, Ar–H⁵ × 2), 7.08 (2H, d, *J* = 16.2 Hz, CO–CH=C × 2), 6.98 (2H, t, *J* = 8.4 Hz, Ar–H⁴ × 2), 5.35 (2H, s, –OH × 2), 3.93 (6H, s, Ar–OCH₃ × 2). ESI-MS *m/z*: 324.9 (M – H)[–], calcd for C₁₉H₁₈O₅: 326.34.

4.1.15. (1*E*,4*E*)-1,5-Bis(2-fluoro-6-(trifluoromethyl)phenyl)penta-1,4-dien-3-one (**B78**)

Yellow powder, 65.2% yield, mp 89.4–92.1 °C. ¹H NMR (CDCl₃) δ: 8.11 (2H, d, *J* = 16.2 Hz, Ar–CH=C × 2), 7.56 (2H, m, Ar–H⁵ × 2), 7.25–7.29 (4H, t, Ar–H^{3,4} × 2), 6.89 (2H, d, *J* = 16.2 Hz, CO–CH=C × 2). ESI-MS *m/z*: 429.4 (M + Na)⁺, calcd for C₁₉H₁₀F₈O: 406.27.

4.1.16. (1*E*,4*E*)-1,5-Bis(5-bromo-2-ethoxyphenyl)penta-1,4-dien-3-one (**B82**)

Yellow powder, 73.1% yield, mp 132.45–134.55 °C. ¹H NMR (CDCl₃) δ: 7.95 (2H, d, 16.2 Hz, Ar–CH=C × 2), 7.69 (2H, d, *J* = 1.8 Hz, Ar–H⁶ × 2), 7.41 (2H, dd, *J* = 1.8 Hz, *J* = 8.4 Hz, Ar–H⁴ × 2), 7.14 (2H, d, *J* = 16.2 Hz, CO–CH=C × 2), 6.80 (2H, d, *J* = 8.4 Hz, Ar–H³ × 2), 4.11 (4H, m, –OCH₂ × 2), 1.45 (6H, s, –CH₃ × 2). ESI-MS *m/z*: 480.8 (M + H)⁺, calcd for C₂₁H₂₀Br₂O₃: 480.19.

4.1.17. (1*E*,4*E*)-1,5-Bis(2-fluoro-4-methoxyphenyl)penta-1,4-dien-3-one (**B84**) [37]

Yellow powder, 52% yield, mp 123.2–124.5 °C. ¹H NMR (CDCl₃) δ: 7.79 (2H, d, *J* = 16.2 Hz, Ar–CH=C × 2), 7.55 (2H, t, *J* = 8.7 Hz,

Ar–H⁶ × 2), 7.05 (2H, d, *J* = 16.2 Hz, CO–CH=C × 2), 6.75 (2H, dd, *J* = 8.4 Hz, *J* = 8.4 Hz, Ar–H³ × 2), 6.66 (2H, dd, *J* = 1.8 Hz, *J* = 8.4 Hz, Ar–H⁵ × 2), 3.85 (6H, s, Ar–OCH₃ × 2). ESI-MS *m/z*: 331.6 (M + H)⁺, calcd for C₁₉H₁₆F₂O₃: 330.33.

4.1.18. (1*E*,4*E*)-1,5-Bis(2,4,5-trimethoxyphenyl)penta-1,4-dien-3-one (**B86**) [38]

Orange powder, 58% yield, mp 173.1–174.8 °C. ¹H NMR (CDCl₃) δ: 8.03 (2H, d, *J* = 15.6 Hz, Ar–CH=C × 2), 7.13 (2H, s, Ar–H⁶ × 2), 7.02 (2H, d, *J* = 16.2 Hz, CO–CH=C × 2), 6.52 (2H, s, Ar–H³ × 2), 3.94 (6H, s, Ar–OCH₃ × 2), 3.90 (12H, s, Ar^{4,5}–OCH₃ × 4). ESI-MS *m/z*: 415.9 (M + H)⁺, calcd for C₂₃H₂₆O₇: 414.45.

4.1.19. (1*E*,4*E*)-1,5-Bis(4-(diethylamino)phenyl)penta-1,4-dien-3-one (**BN1**) [35]

Brick red powder, 50.9% yield, mp 155.5–157.8 °C. ESI-MS *m/z*: 377.2 (M + H)⁺, calcd for C₂₅H₃₂N₂O: 376.53.

4.1.20. (1*E*,4*E*)-1,5-Bis(4-(piperidin-1-yl)phenyl)penta-1,4-dien-3-one (**BN2**)

Orange powder, 41.2% yield, mp 181.2–184.9 °C. ¹H NMR (CDCl₃) δ: 7.75 (2H, d, *J* = 16.2 Hz, Ar–CH=C × 2), 7.53 (4H, d, *J* = 9.0 Hz, Ar–H^{2,6} × 2), 6.95 (2H, d, *J* = 16.2 Hz, CO–CH=C × 2), 6.92 (4H, d, *J* = 4.8 Hz, Ar–H^{3,5} × 2), 3.33 (8H, t, *J* = 5.4 Hz, N–CH₂ × 4), 1.72 (4H, s, >CH₂ × 2), 1.67 (8H, d, *J* = 4.8 Hz, CH₂–C–CH₂ × 6). ESI-MS *m/z*: 401.3 (M + H)⁺, calcd for C₂₇H₃₂N₂O: 400.56.

4.1.21. (1*E*,4*E*)-1,5-Bis(4-morpholinophenyl)penta-1,4-dien-3-one (**BN3**)

Orange powder, 92.5% yield, mp 215.1–217.0 °C. ¹H NMR (CDCl₃) δ: 7.70 (2H, d, *J* = 15.6 Hz, Ar–CH=C × 2), 7.49 (4H, d, *J* = 8.4 Hz, Ar–H^{2,6} × 2), 6.95 (2H, d, *J* = 15.6 Hz, CO–CH=C × 2), 6.92 (4H, t, *J* = 9.0 Hz, Ar–H^{3,5} × 2), 3.89 (8H, t, *J* = 4.8 Hz, O–CH₂ × 4), 3.29 (8H, t, *J* = 4.8 Hz, N–CH₂ × 4). ESI-MS *m/z*: 405.3 (M + H)⁺, calcd for C₂₅H₂₈N₂O₃: 404.5.

4.1.22. (1*E*,4*E*)-1,5-Bis(4-(bis(2-chloroethyl)amino)phenyl)penta-1,4-dien-3-one (**BN4**)

Yellow powder, 74.6% yield, mp 197.4–203.0 °C. ¹H NMR (CDCl₃) δ: 7.67 (2H, d, *J* = 15.6 Hz, Ar–CH=C × 2), 7.54 (4H, d, *J* = 8.4 Hz, Ar–H^{2,6} × 2), 6.90 (2H, d, *J* = 15.6 Hz, CO–CH=C × 2), 6.57 (4H, d, *J* = 8.4 Hz, Ar–H^{3,5} × 2), 3.81 (8H, m, N–CH₂ × 4), 3.65 (8H, m, Cl–CH₂ × 4). ESI-MS *m/z*: 515.1 (M + H)⁺, calcd for C₂₇H₃₀Cl₄N₂O: 514.31.

4.1.23. (2*E*,6*E*)-2,6-Bis(2-fluoro-3-(trifluoromethyl)benzylidene)cyclohexanone (**C77**)

Yellow powder, 62.5% yield, mp 119.7–122.3 °C. ¹H NMR (CDCl₃) δ: 7.78 (2H, s, Ar–CH=C × 2), 7.60 (2H, t, *J* = 7.2 Hz, Ar–H⁴ × 2), 7.55 (2H, t, *J* = 7.2 Hz, Ar–H⁶ × 2), 7.27 (2H, t, *J* = 7.2 Hz, Ar–H⁵ × 2), 2.78 (4H, t, *J* = 5.6 Hz, CH₂–C–CH₂), 1.79 (2H, m, >CH₂). ESI-MS *m/z*: 447.2 (M + H)⁺, calcd for C₂₂H₁₄F₈O: 446.33.

4.1.24. (2*E*,6*E*)-2,6-Bis(2-fluoro-6-(trifluoromethyl)benzylidene)cyclohexanone (**C78**)

Yellow powder, 56.5% yield, mp 114.9–116.7 °C. ¹H NMR (CDCl₃) δ: 7.62 (2H, s, Ar–CH=C × 2), 7.53 (2H, d, *J* = 8.4 Hz, Ar–H⁵ × 2), 7.44 (2H, dd, *J* = 8.4 Hz, *J* = 8.4 Hz, Ar–H⁴ × 2), 7.31 (2H, t, *J* = 8.4 Hz, Ar–H³ × 2), 2.45 (4H, t, *J* = 6.3 Hz, CH₂–C–CH₂), 1.69 (2H, m, >CH₂). ESI-MS *m/z*: 447.2 (M + H)⁺, 469.0 (M + Na)⁺, calcd for C₂₂H₁₄F₈O: 446.33.

4.1.25. (2*E*,6*E*)-2,6-Bis(2-fluoro-4-(trifluoromethyl)benzylidene)cyclohexanone (**C80**)

Yellow powder, 88.5% yield, mp 145.4–147.7 °C. ¹H NMR (CDCl₃) δ: 7.78 (2H, s, Ar–CH=C × 2), 7.48 (2H, t, *J* = 7.8 Hz, Ar–H⁵ × 2), 7.45

(2H, d, $J = 8.4$ Hz, Ar–H⁶ × 2), 7.39 (2H, d, $J = 9.6$ Hz, Ar–H³ × 2), 2.81 (4H, t, $J = 6.0$ Hz, CH₂–C–CH₂), 1.80 (2H, m, >CH₂). ESI-MS m/z : 445.7 (M – H)[–], calcd for C₂₂H₁₄F₈O: 446.33.

4.1.26. (2*E*,6*E*)-2,6-Bis(2-fluoro-5-methoxy benzylidene) cyclohexanone (**C81**)

Yellow powder, 58.3% yield, mp 91.3–93.4 °C. ¹H NMR (CDCl₃) δ: 7.77 (2H, s, Ar–CH=C × 2), 7.03 (2H, t, $J = 9.0$ Hz, Ar–H³ × 2), 6.83–6.87 (4H, m, Ar–H^{4,6} × 2), 3.80 (6H, s, Ar–OCH₃ × 2), 2.81 (4H, t, $J = 5.4$ Hz, CH₂–C–CH₂), 1.78 (2H, m, >CH₂). ESI-MS m/z : 371.0 (M + H)⁺, calcd for C₂₂H₂₀F₂O₃: 370.39.

4.1.27. (2*E*,6*E*)-2,6-Bis(5-bromo-2-ethoxy benzylidene) cyclohexanone (**C82**)

Yellow powder, 91.1% yield, mp 136.5–138.14 °C. ¹H NMR (CDCl₃) δ: 7.89 (2H, s, Ar–CH=C × 2), 7.4 (2H, d, $J = 2.4$ Hz, Ar–H⁶ × 2), 7.38 (2H, d, $J = 2.4$ Hz, $J = 9.0$ Hz, Ar–H⁴ × 2), 6.78 (2H, d, $J = 9.0$ Hz, Ar–H³ × 2), 4.05 (4H, m, –OCH₂ × 2), 2.83 (4H, t, $J = 5.4$ Hz, CH₂–C–CH₂), 1.78 (2H, m, >CH₂), 1.42 (6H, m, CH₃ × 2). ESI-MS m/z : 520.8 (M + H)⁺, calcd for C₂₄H₂₄Br₂O₃: 520.25.

4.1.28. (2*E*,6*E*)-2,6-Bis(2,4,5-trimethoxybenzylidene)cyclohexanone (**C86**)

Yellow powder, 62% yield, mp 121.2–123.6 °C. ¹H NMR (CDCl₃) δ: 7.97 (2H, s, Ar–CH=C × 2), 6.91 (2H, s, Ar–H⁶ × 2), 6.53 (2H, s, Ar–H³ × 2), 3.84 (18H, s, Ar–OCH₃ × 6), 2.85 (4H, t, $J = 4.8$ Hz, CH₂–C–CH₂), 1.78 (2H, m, >CH₂). ESI-MS m/z : 455.1 (M + H)⁺, calcd for C₂₆H₃₀O₇: 454.51.

4.1.29. (2*E*,6*E*)-2,6-Bis(2,4-bis(trifluoromethyl)benzylidene) cyclohexanone (**C87**)

Yellow powder, 91% yield, mp 129.1–130.8 °C. ¹H NMR (CDCl₃) δ: 7.98 (2H, s, Ar–H² × 2), 7.91 (2H, s, Ar–CH=C × 2), 7.83 (2H, d, $J = 7.8$ Hz, Ar–H⁵ × 2), 7.47 (2H, d, $J = 8.4$ Hz, Ar–H⁶ × 2), 2.60 (2H, t, $J = 5.1$ Hz, CH₂–C–CH₂), 1.73 (2H, m, >CH₂). ESI-MS m/z : 547.9 (M + H)⁺, calcd for C₂₄H₁₄F₁₂O: 546.35.

4.1.30. (2*E*,6*E*)-2,6-Bis(4-(diethylamino)benzylidene) cyclohexanone (**CN1**) [35]

Brick red powder, 21.4% yield, mp 143.7–145.2 °C. ESI-MS m/z : 417.4 (M + H)⁺, calcd for C₂₈H₃₆N₂O: 416.6.

4.1.31. (2*E*,6*E*)-2,6-Bis(4-(piperidin-1-yl)benzylidene) cyclohexanone (**CN2**)

Yellow powder, 72.4% yield, mp 230.4–233.6 °C [230–232 °C, lit. [36]]. ESI-MS m/z : 441.4 (M + H)⁺, calcd for C₂₈H₃₆N₂O: 440.62.

4.1.32. (2*E*,6*E*)-2,6-Bis(4-morpholinobenzylidene)cyclohexanone (**CN3**)

Yellow powder, 22% yield, mp 234.3–237.1 °C. ¹H NMR (CDCl₃) δ: 7.77 (2H, s, Ar–CH=C × 2), 7.47 (4H, d, $J = 9.0$ Hz, Ar–H^{2,6} × 2), 6.94 (4H, d, $J = 8.4$ Hz, Ar–H^{3,5} × 2), 3.90 (8H, d, $J = 4.2$ Hz, O–CH₂ × 4), 3.27 (8H, t, $J = 4.2$ Hz, N–CH₂ × 4), 2.95 (4H, s, –CH₂–CH₂), 1.60 (2H, m, >CH₂). ESI-MS m/z : 445.3 (M + H)⁺, calcd for C₂₈H₃₂N₂O₃: 444.57.

4.1.33. (2*E*,6*E*)-2,6-Bis(4-(bis(2-chloroethyl)amino)benzylidene) cyclohexanone (**CN4**)

Yellow powder, 87.2% yield, mp 201.4–204.2 °C. ¹H NMR (CDCl₃) δ: 7.77 (4H, m, Ar–H^{2,6} × 2), 7.45 (2H, m, Ar–CH=C × 2), 6.68–6.76 (4H, m, Ar–H^{3,5} × 2), 3.77–3.86 (8H, m, N–CH₂ × 4), 3.64–3.69 (8H, m, Cl–CH₂ × 4), 2.92 (4H, m, CH₂–CH₂), 1.81 (2H, s, >CH₂). ESI-MS m/z : 555.7 (M + H)⁺, calcd for C₂₇H₃₀Cl₄N₂O: 554.38.

4.2. Cell line and reagents

Mouse RAW 264.7 macrophages were obtained from the American Type Culture Collection (ATCC, USA). Cell culture reagents were obtained from Gibco. Fetal bovine serum was from HyClone and was heat-inactivated for 30 min at 65 °C. LPS purchased from Sigma was dissolved in PBS. Curcumin and its analogues were dissolved in DMSO before use.

4.3. Cell treatment and ELISA assay [32,33]

Mouse RAW 264.7 macrophages were incubated in DMEM media (Gibco) supplemented with 10% FBS, 100 U/ml penicillin, and 100 μg/ml streptomycin at 37 °C with 5% CO₂. Cells were pre-treated with 10 μM of curcumin, analogues or vehicle control for 2 h, then treated with LPS (0.5 μg/ml) for 22 h. After treatment, the culture media and cells were collected separately. The culture media collected were centrifuged at 1000 rpm for 10 min. The levels of TNF-α and IL-6 in the media were determined by ELISA using mouse TNF-α and mouse IL-6 ELISA Kits (BOSTER, USA). After centrifugation, the supernatant was separated and stored at –70 °C until use. Cells were washed with PBS and harvested with cell lysis buffer (Tris–HCl 20 mM, NP40 1%, NaCl 150 mM, EDTA 2 mM, Na₃VO₄ 200 mM, SDS 0.1%, NaF 20 mM). The mixed liquor was shaken vigorously for 10 min in lysis buffer at 0 °C. After being centrifuged at 12,000 rpm for 5 min at 4 °C, the total protein was collected and the concentrations were determined using Bio-Rad protein assay reagents. The total amount of the inflammatory factor in the media was normalized to the total protein amount of the viable cell pellets.

4.4. Conventional quantum chemical descriptors

$E_{\text{HOMO}}/E_{\text{LUMO}}$: energy of the highest occupied molecular orbital (E_{HOMO}) and energy of the lowest unoccupied molecular orbital (E_{LUMO}); ΔE : orbital energy gap between HOMO and LUMO ($E_{\text{LUMO}} - E_{\text{HOMO}}$); Q_A : net atomic charge on atom A; F_r^E/F_r^N : indices of frontier electron density, $F_r^E = f_r^E/E_{\text{HOMO}}$, $F_r^N = f_r^N/E_{\text{LUMO}}$, where f_r^E and f_r^N are the electrophilic and nucleophilic atomic frontier electron densities, respectively; q_π : the sum of π electron densities of all atoms; SDE/SDN: the sum of electrophilic and nucleophilic superdelocalizabilities. In order to better represent quantitatively the contributions of these orbitals in two distinct parts of the molecules, SDE-BS/SDN-BS and SDE-sub/SDN-sub were calculated over the basic structure moiety and the variable radical moiety [39].

4.5. Calculation method and models

Initially, full geometric optimization of the 33 molecules was performed using DFT/B3LYP methods with the 6-31G(d) basis sets. All molecular orbitals are calculated by the Firefly QC package, which is partially based on the GAMESS (US) source code. Based on these precise quantum chemical descriptors, a quantitative structure–activity relationships study has been carried out. The QSAR equations and statistics were calculated with the open-source R framework, a powerful tool for statistical computing and graphics [39,40].

Acknowledgment

This work was supported by the National Natural Science Funding of China (20802054), Young Talent Funding of Zhejiang Department of Health (2009QN020), Key Project of Wenzhou Sci&Tech Bureau (Y20090009 & Y20100006) and Zhejiang Natural Science Funding (Y20101108).

Appendix. Supplementary material

Supplementary data related to this article can be found online at doi:10.1016/j.ejmech.2010.09.037.

References

- [1] B.V. Reddy, J.S. Sundari, E. Balamurugan, V.P. Menon, *Mol. Cell. Biochem.* 331 (2009) 127–133.
- [2] G. O'Sullivan-Coyne, G.C. O'Sullivan, T.R. O'Donovan, K. Piwocka, S.L. McKenna, *Br. J. Cancer* 101 (2009) 1585–1595.
- [3] B.B. Aggarwal, A. Kumar, A.C. Bharti, *Anticancer Res.* 23 (2003) 363–398.
- [4] X.Y. Qin, Y. Cheng, L.C. Yu, *Neurosci. Lett.* 480 (2010) 21–24.
- [5] S.A. Marathe, S. Ray, D. Chakravorty, *PLoS One* 5 (2010) e11511.
- [6] M. Boonrao, S. Yodkeeree, C. Ampasavate, S. Anuchapreeda, P. Limtrakul, *Arch. Pharm. Res.* 33 (2010) 989–998.
- [7] P. Rafiee, V.M. Nelson, S. Manley, M. Wellner, M. Floer, D.G. Binion, R. Shaker, *Am. J. Physiol. Gastrointest. Liver Physiol.* 296 (2009) G388–G398.
- [8] T. Morimoto, Y. Sunagawa, T. Kawamura, T. Takaya, H. Wada, A. Nagasawa, M. Kameda, M. Fujita, A. Shimatsu, T. Kita, K. Hasegawa, *J. Clin. Invest.* 118 (2008) 868–878.
- [9] A.M. Siddiqui, X. Cui, R. Wu, W. Dong, M. Zhou, M. Hu, H.H. Simms, P. Wang, *Crit. Care Med.* 34 (2006) 1874–1882.
- [10] B.Y. Kang, S.W. Chung, W. Chung, S. Im, S.Y. Hwang, T.S. Kim, *Eur. J. Pharmacol.* 384 (1999) 191–195.
- [11] J.S. Jurenka, *Altern. Med. Rev.* 14 (2009) 141–153.
- [12] C.H. Hsu, A.L. Cheng, *Adv. Exp. Med. Biol.* 595 (2007) 471–480.
- [13] F. Di Mario, L.G. Cavallaro, A. Nouvenne, N. Stefani, G.M. Cavestro, V. Iori, M. Maino, G. Comparato, L. Fanigliulo, E. Morana, A. Pilotto, L. Martelli, M. Martelli, G. Leandro, A. Franze, *Helicobacter* 12 (2007) 238–243.
- [14] M. Bayet-Robert, F. Kwiatkowski, M. Leheurteur, F. Gachon, E. Planchat, C. Abrial, M.A. Mouret-Reynier, X. Durando, C. Barthelemy, P. Chollet, *Cancer Biol. Ther.* 9 (2010) 8–14.
- [15] M.H. Pan, T.M. Huang, J.K. Lin, *Drug Metab. Dispos.* 27 (1999) 486–494.
- [16] G. Bar-Sela, R. Epelbaum, M. Schaffer, *Curr. Med. Chem.* 17 (2010) 190–197.
- [17] G. Garcea, D.J. Jones, R. Singh, A.R. Dennison, P.B. Farmer, R.A. Sharma, W.P. Steward, A.J. Gescher, D.P. Berry, *Br. J. Cancer* 90 (2004) 1011–1015.
- [18] M.J. Rosemond, L. St John-Williams, T. Yamaguchi, T. Fujishita, J.S. Walsh, *Chem. Biol. Interact.* 147 (2004) 129–139.
- [19] Y.J. Wang, M.H. Pan, A.L. Cheng, L.I. Lin, Y.S. Ho, C.Y. Hsieh, J.K. Lin, *J. Pharm. Biomed. Anal.* 15 (1997) 1867–1876.
- [20] G. Liang, L. Shao, Y. Wang, C. Zhao, Y. Chu, J. Xiao, Y. Zhao, X. Li, S. Yang, *Bioorg. Med. Chem.* 17 (2009) 2623–2631.
- [21] I.B. McInnes, G. Schett, *Nat. Rev. Immunol.* 7 (2007) 429–442.
- [22] I. Cohen, P. Rider, Y. Carmi, A. Braiman, S. Dotan, M.R. White, E. Voronov, M.U. Martin, C.A. Dinarello, R.N. Apte, *Proc. Natl. Acad. Sci. U.S.A.* 107 (2010) 2574–2579.
- [23] M. Ammirante, J.L. Luo, S. Grivennikov, S. Nedospasov, M. Karin, *Nature* 464 (2010) 302–305.
- [24] J. Navarro-Gonzalez, C. Mora-Fernandez, M. Gomez-Chinchon, M. Muros, H. Herrera, J. Garcia, *Int. J. Immunopathol. Pharmacol.* 23 (2010) 51–59.
- [25] A. Kalogeropoulos, V. Georgiopoulou, B.M. Psaty, N. Rodondi, A.L. Smith, D.G. Harrison, Y. Liu, U. Hoffmann, D.C. Bauer, A.B. Newman, S.B. Kritchevsky, T.B. Harris, J. Butler, *J. Am. Coll. Cardiol.* 55 (2010) 2129–2137.
- [26] Y. Hu, G. Tong, W. Xu, J. Pan, K. Ryan, R. Yang, A.R. Shuldiner, D.W. Gong, D. Zhu, *Diab Vasc. Dis. Res.* 6 (2009) 262–268.
- [27] Y. Qiu, T. Yanase, H. Hu, T. Tanaka, Y. Nishi, M. Liu, K. Sueishi, T. Sawamura, H. Nawata, *Endocrinology* 151 (2010) 3307–3316.
- [28] R. Mazon, O. Itzhaki, S. Sela, Y. Yagil, M. Cohen-Mazor, C. Yagil, B. Kristal, *Hypertension* 55 (2010) 353–362.
- [29] S.K. Jain, J. Rains, J. Croad, B. Larson, K. Jones, *Antioxid. Redox Signal.* 11 (2009) 241–249.
- [30] Y. Moon, W.C. Glasgow, T.E. Eling, *J. Pharmacol. Exp. Ther.* 315 (2005) 788–795.
- [31] J. Lee, Y.H. Im, H.H. Jung, J.H. Kim, J.O. Park, K. Kim, W.S. Kim, J.S. Ahn, C.W. Jung, Y.S. Park, W.K. Kang, K. Park, *Biochem. Biophys. Res. Commun.* 334 (2005) 313–318.
- [32] G. Liang, H. Zhou, Y. Wang, E.C. Gurley, B. Feng, L. Chen, J. Xiao, S. Yang, X. Li, J. Cell. Mol. Med. 13 (2009) 3370–3379.
- [33] G. Liang, X. Li, L. Chen, S. Yang, X. Wu, E. Studer, E. Gurley, P.B. Hylemon, F. Ye, Y. Li, H. Zhou, *Bioorg. Med. Chem. Lett.* 18 (2008) 1525–1529.
- [34] G. Liang, S. Yang, L. Jiang, Y. Zhao, L. Shao, J. Xiao, F. Ye, Y. Li, X. Li, *Chem. Pharm. Bull. (Tokyo)* 56 (2008) 162–167.
- [35] K. Yamashita, S. Imahashi, S. Ito, *Dyes Pigm.* 76 (2008) 748–753.
- [36] A. Basta, A. Girgis, H. El-Saied, *Dyes Pigm.* 54 (2002) 1–10.
- [37] K.H. Lee, F.H. Ab Aziz, A. Syahida, F. Abas, K. Shaari, D.A. Israfil, N.H. Lajis, *Eur. J. Med. Chem.* 44 (2009) 3195–3200.
- [38] H. Yamakoshi, H. Otori, C. Kudo, A. Sato, N. Kanoh, C. Ishioka, H. Shibata, Y. Iwabuchi, *Bioorg. Med. Chem.* 18 (2010) 1083–1092.
- [39] J. Sullivan, A. Jones, K. Tanji, *J. Chem. Inf. Comput. Sci.* 40 (2000) 1113–1127.
- [40] M. Schmidt, K. Baldrige, J. Boatz, S. Elbert, M. Gordon, J. Jensen, S. Koseki, N. Matsunaga, K. Nguyen, S. Su, *J. Comput. Chem.* 14 (1993) 1347–1363.